Proceedings of ASME Turbo Expo 2024
Turbomachinery Technical Conference and Exposition
GT2024
June 24-28, 2024, London, England

GT2024-121641

NASA HECC GEOMETRY AND PERFORMANCE REVIEW PART 3: A NUMERICAL AND EXPERIMENTAL INVESTIGATION OF TIP CLEARANCE EFFECTS ON THE VANELESS DIFFUSER CONFIGURATION

Herbert M. Harrison[1], Tammy Nguyen-Huynh[1,2], Randall M. Mathison[2]

[1]NASA Glenn Research Center, Cleveland, OH
[2]The Ohio State University, Columbus, OH

ABSTRACT

Tip clearance effects in centrifugal compressors have been extensively investigated to understand the losses associated with the flow in the impeller tip clearance gap between the rotating blades and the stationary shroud. In Part 3 of this multipart investigation, experimental data and validated numerical simulations from Parts 1 and 2 were used to analyze the effects of the size of the tip clearance gap on the High Efficiency Centrifugal Compressor performance and aerodynamics. Four tip clearance gaps ranging from 0.012-in to 0.030-in (2.0% to 4.9% of the impeller exit blade height) were considered at both design and off-design operating conditions. The total pressure ratio and efficiency of the stage are found to decay linearly with increasing tip gaps. The sensitivity of the impeller performance to the tip gap was found to vary with the rotational speed of the compressor. Spanwise surveys of flow angle, total pressure, and total temperature collected at the impeller exit at design speed are used to validate numerical simulations at each experimental tip gap condition. Numerical simulations show that increased turbulence kinetic energy near the shroud at larger tip gaps leads to spanwise mixing of high entropy fluid near the impeller trailing edge which decreases the useful work input by the impeller. The data presented have been made available to the public in the HECC Data Archive located at https://storage.googleapis.com/hecc-data/NASA-HECC-Data-Archive.zip.

Keywords: centrifugal compressor, impeller, tip clearance

NOMENCLATURE

B	performance parameter
CR	clearance ratio
h_0	stagnation enthalpy
$HECC$	High Efficiency Centrifugal Compressor
k	performance parameter sensitivity
$\dot{m}_c$	inlet corrected mass flow rate
P_0	stagnation pressure
T_0	stagnation temperature
TC	tip clearance
TCR	tip clearance ratio
TDC	top dead center
TPR	total pressure ratio
TTR	total temperature rise ratio

SUBSCRIPTS

0	inlet rating station
3	impeller exit rating station
s	isentropic process condition

1. INTRODUCTION

Losses resulting from tip clearance flows in rotating turbomachinery contribute significantly to the overall losses in gas turbine engines and their components. The demand for more efficient gas turbine engines has consistently resulted in a push for smaller engine cores which is often achieved through a reduction in blade height. The decreased blade heights have, in turn, resulted in greater relative importance of the tip clearance flow as the tip gap between the rotating and stationary components remains unchanged. An improved understanding of the tip clearance flow in gas turbine compressors is needed to support future designs in which the tip clearance flow has outsized roles in the overall efficiency of gas turbine engines, particularly in centrifugal compressors, which support the low exit corrected mass flow rate design space.

Previous research on the effects of tip clearance in centrifugal compressors has often focused on the adverse effects of increasing tip clearance on the stage performance. Senoo and Ishida's [1] model for the drop in input head with increasing tip clearance lists the relation as being linear and proportional to the cotangent of the impeller exit blade angle. Comparisons of the model's prediction to previously observed experimental results in the literature matched well. Brasz's [2] experiment on a centrifugal compressor stage with a vaneless diffuser yielded a similar trend to what Senoo and Ishida predicted. However, the relationship between the work input coefficient and size of the tip gap was nonlinear at smaller tip clearances (clearance ratios less than 6%) as work input was found to be more sensitive for

those conditions. Ishida et al. [3] later performed a study on a pair of centrifugal impellers with and without backswept blades to investigate impeller exit velocity distribution. They found that input power remained nearly unchanged for the impeller with radial blades with increasing tip clearance, while input power decreased for the impeller with backswept blades. This reduction in input power was observed to be linear. The relationship remained linear with similar slope values at all mass flow rates considered within the scope of the study. In contrast, other researchers, such as Tang et al. [4], observed minimal changes in work input and total enthalpy rise with varying tip clearance in a centrifugal compressor with vaneless diffuser. When investigating the effects of variable tip clearance at different mass flow rates along a given speedline, they saw that work input increases and total enthalpy rise decreases with increasing mass flow. Wilkosz et al. [5] studied a centrifugal compressor stage with a pipe diffuser and attained experimental results that also showed minimal effects of variable tip clearance on total temperature ratio. In an investigation with a transonic centrifugal compressor with a vaned diffuser, Fuehne et al. [6] found similar results in terms of the sensitivity of the stage work factor to changes in tip clearance. The work input was less sensitive to tip clearance relative to other stage performance parameters, and the relationship of the investigated performance parameters with the size of the tip gap were not heavily dependent on the impeller tip relative Mach number.

Findings for tip clearance effects on a compressor's stage total pressure ratio tend to reach a consensus: the stage total pressure ratio decreases with increasing tip clearance [2,4–7]. In Brasz's case [2], the sensitivity of stage total pressure ratio is greater at smaller tip clearances, similar to the trend seen with work input for the same study. This concurs with the trend observed in the numerical results presented by Tang et al. [4]. Eum and Kang [7] examined tip clearance effects on a compressor with a vaned diffuser and found the variation of total pressure ratio with increasing tip clearance was linear. Turunen-Saaresti and Jaatinen [8] analyzed the influence of different compressor features on tip clearance effects for six centrifugal compressors found in the literature and observed similar linear relationships between tip clearance and performance for each of the considered compressors. However, the constant of proportionality differed between compressors. Fuehne et al. [6] found that the transition to a transonic condition sharply increased the sensitivity of total pressure ratio to changes in tip clearance.

As is common in turbomachinery research, understanding the effect of the tip gap size on efficiency has been a primary driver of centrifugal compressor tip clearance investigations. Efficiency generally decreases with increasing tip clearance. Mashimo et al. [9] analyzed a shrouded and an unshrouded impeller to understand the effects of tip clearance on efficiency at different operating conditions. Efficiency was seen to be more sensitive to changes in tip clearance at larger mass flow rates, and these results have been corroborated by other researchers [4]. Tang et al., along with numerous other researchers [5–8], note that efficiency sensitivity to variable tip clearance is linear. Fuehne et al. [6] observed that this sensitivity peaked as the impeller reached transonic conditions.

Significant effort has been expended over the past decades to predict or estimate the losses accrued by secondary flows associated with the tip clearance gap through various modeling approaches. One dimensional loss models for use in the design phase, such as the expression for leakage loss developed by Mashimo et al. [9], is an example. Senoo and Ishida [1,10] theorized that there are two components which contribute to losses from the tip clearance gap: the pressure loss from tip leakage flow across the blade and the pressure loss associated with the layer of low momentum fluid along the shroud. From this approach, Senoo and Ishida developed expressions to describe the efficiency reduction and pressure loss associated with the tip clearance using empirical coefficients [10]. Eum and Kang's study [7] described the loss distribution resulting from the tip clearance flow using a loss factor in terms of entropy generation in addition to models for work input and entropy generation. Turunen-Saaresti and Jaatinen [8] considered the effect of various features such as blade number, blade height ratio, diffusion ratio, and specific speed on efficiency and found no correlation between these features and stage performance reduction.

This study contributes to the current understanding of loss arising from the tip clearance flow by examining the underlying flow mechanisms within the impeller. The effects of tip clearance on the performance of a high-speed centrifugal compressor impeller with a vaneless diffuser were analyzed experimentally and computationally as part of this effort. A validated numerical model was used to develop an understanding of the underlying flow mechanisms that contribute to reduced compressor performance at large tip gaps. The experimental data presented in this paper, as well as the compressor geometry and operating conditions needed to replicate the numerical simulations, is non-normalized and has been made publicly available for further investigation.

2. FACILITY AND INSTRUMENTATION

The data for this investigation were obtained from High Efficiency Centrifugal Compressor (HECC) which is housed and tested in the NASA Small Engine Components Compressor Test Facility at NASA Glenn Research Center. Multiple configurations of the HECC stage have been developed since the initial test program began in the early 2010s. Extensive documentation on the development of the HECC vaned diffuser stage is given by Medic et al. [11], and details of the facility and the vaneless diffuser configuration are documented by Harrison et al. [12]. Additionally, the geometry, performance, and aerodynamic measurements for all published HECC data are available in the HECC Data Archive [13].

For the present work the baseline plastic inlet, HECC impeller, and vaneless diffuser components were used, Figure 1. The baseline plastic inlet is an exact replica of the original metal inlet designed for the stage but was additively manufactured from Stratasys acrylonitrile styrene acrylate to investigate the effect of various inlet configurations on centrifugal compressor

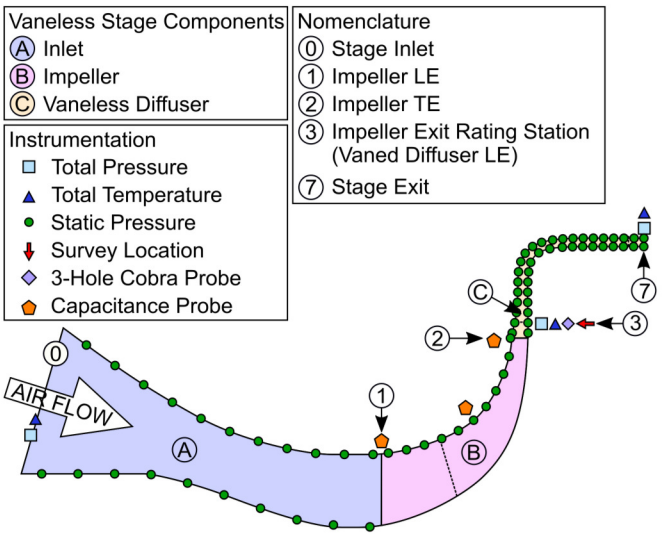

FIGURE 1. HECC VANELESS DIFFUSER COMPONENTS, NOMENCLATURE, AND INSTRUMENTATION.

performance. The HECC impeller is scaled to approximately twice the size of flight hardware, has 15 main blades and 15 splitter blades with 30 degrees of backsweep at the trailing edge. The vaneless diffuser was designed to provide the impeller with design intent exit conditions to better understand the characteristics of the impeller exit flow. The vaneless diffuser features a 30% shroud side pinch which extends from the impeller trailing edge to a radius ratio of 1.12 based on the impeller trailing edge radius. Following the pinch, the area of the vaneless diffuser is approximately constant up to the entrance of bend to axial. To maintain the constant area flow path downstream of the pinch, the span decreases by approximately 11.7% from the termination of the pinch at radius ratio 1.12 to the entrance of the bend at radius ratio 1.26.

The design point of the vaneless diffuser configuration is 21,789-rpm and 11-lbm/s at standard day conditions. At design point, the machine provides a stage total pressure ratio (TPR) of 4.55, inlet flow coefficient of 0.044, and loading coefficient of 0.78. At 100% corrected speed, the machine Mach number is 1.45 and the impeller tip relative Mach number enters the transonic regime. The design intent tip clearance gap is 2.0% of the impeller exit blade height in terms of tip clearance ratio (TCR), or 0.012-in, at the impeller trailing edge.

Data are acquired with the in-house NASA COBRA system. Steady pressure measurements are obtained with Netscanner 9816 modules paired with Netscanner 98RK-1 chassis or Druck UNIK 5000 pressure transducers with uncertainties 0.15% and 0.04%, respectively. Temperatures are recorded to within 4°F with K-type thermocouples and Scanivalve DTS 4050 units. An ASME standard orifice plate is used to measure the mass flow rate through the machine to within 1% at all operating conditions, and feedback control from the variable frequency power system maintains rotational speed with 0.013% of the setpoint.

In addition to the meridional view of the primary flow path, the relevant instrumentation for the tip clearance investigation discussed in the present work are shown in Figure 1. Performance of the stage and impeller are characterized with total pressure and total temperature measurements located upstream of the inlet duct in the settling chamber, at the impeller exit rating station, and at the stage exit (stations 0, 3, and 7, respectively, in Figure 1). The impeller exit rating station is located just downstream of the impeller trailing edge at a radius ratio of 1.072. Shroud access ports, also located at the impeller exit rating station, allow for traversal of 3-hole cobra probes and total temperature probes across the vaneless diffuser span for detailed characterization of the impeller exit flow. Static pressure taps are located throughout the hub and shroud of the flow path, with the greatest concentration of measurements in the vaneless diffuser.

Tip clearance readings were meticulously recorded given the subject matter of the present investigation. GadCap capacitance probes are located at the leading edge, knee, and trailing edge of the impeller as outlined by the meridional cross section in Figure 1, and the signals were processed to engineering units via the CapaciSense software. Additionally, Figure 2 provides a forward-looking-aft view of the tip clearance data acquisition equipment. While only a single capacitance probe is located at each meridional location, four rub probes are distributed around the circumference of the impeller at the inducer, knee, and exducer, as well. The rub probes are used in conjunction with the capacitance probes during mechanical checkouts both for in situ calibration of the capacitance probes as well as evaluation of the variation in the tip clearance gap around the casing circumference. It should be noted that by their nature rub probes inherently record the smallest tip clearance gap at a given location, whereas the capacitance probes record a gap measurement for each individual blade.

The eccentricity of the impeller relative to the shroud for each rub probe location at 100% corrected speed and design tip clearance condition (2.0% TCR) is also shown in Figure 2. The provided values for eccentricity are relative to the value recorded by the capacitance probe at each meridional location. While the eccentricity is not negligible (nearly 0.005-in), the authors would consider it small relative to both the compressor stage geometry and the scope of the investigation. The impeller trailing edge radius is 8.5-in, and thus the change in tip clearance around the circumference of the stage is less than 0.03% of the stage diameter. Furthermore, the circumferential variation in tip clearance is less than 0.9% of the 0.609-in impeller exit blade height, and the variation is small relative to the range of tip clearance setpoints (2.0% to 3.9% TCR) at which performance and aerodynamic data were acquired. Finally, previous investigations yielded good agreement in aerodynamic measurements around the circumference of the impeller exit [12].

The tip clearance gap is manipulated and actively controlled with a precision stepper motor which axially traverses the impeller to change the axial tip clearance gap at the impeller trailing edge. Axial translation of the impeller results in a

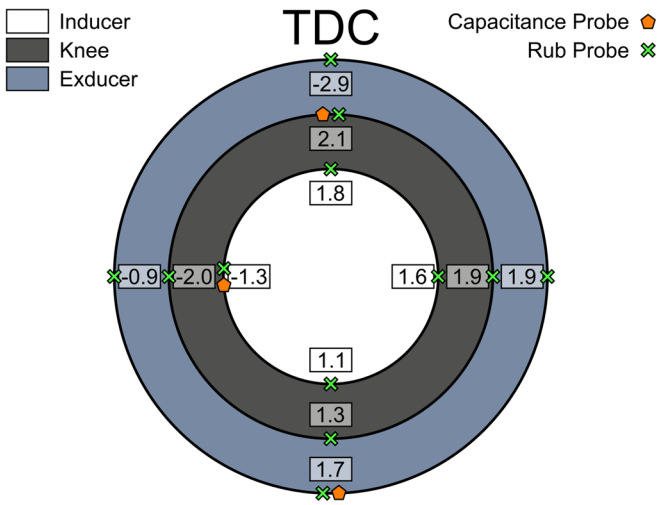

FIGURE 2. FORWARD-LOOKING-AFT ILLUSTRATION OF TIP CLEARANCE INSTRUMENTATION AND TIP GAP ECCENTRICITY IN THOUSANDTHS OF AN INCH AS MEASURED BY RUB PROBES AT 100% CORRECTED SPEED.

variable forward facing step between the vaneless diffuser hub surface and the impeller hub at the trailing edge. As is typical of centrifugal compressor tip clearance studies, the presence of the step is noted but the impact of the step is not considered.

In conjunction with the tip clearance monitoring system, the impeller exit tip clearance is controlled to a precision of 0.0005" at all recorded operating conditions in the present study. Four different tip clearance conditions were tested: 0.012-in (design tip clearance), 0.018-in, 0.024-in, and 0.030-in. These values correspond to clearance ratios of 2.0%, 3.0%, 3.9%, and 4.9%, respectively, based on the impeller exit blade height. The inducer tip clearance was nearly constant with axial movement of the impeller, varying from 0.35% to 0.49% of the inducer leading edge span of 2.65-in.

To characterize the impeller exit flow, spanwise surveys were conducted at open throttle, peak efficiency, and near-stall operating conditions at 75%, 85%, 90%, 95%, and 100% corrected speed. Due to manuscript length constraints, only surveys at 100% are presented. Two calibrated three-hole cobra-style probes 98° apart were used to calculate the flow angle and total pressure at the impeller exit at numerous spanwise locations per the procedure specified by Treaster and Yocum [14]. The resulting values from each probe were generally in good agreement with each other and were therefore averaged to obtain single representative surveys of the quantities at the impeller exit. The calculated values of total pressure obtained from the 3-hole probes were also in good agreement from the total pressure rakes at the impeller exit rating station. Total temperature probes were used in the same manner to acquire total temperature data across the impeller span. Since both the probes and the rakes at the impeller exit are small relative to the large flow area of the vaneless diffuser, the instrumentation is expected to have a negligible effect on blockage and the impeller exit flow [15].

Details of the clearance measurements as well as the aerodynamic and performance data, including the low speed surveys not included in the present work, have been made available in the HECC Data Archive [13].

3. TIP CLEARANCE AND IMPELLER PERFORMANCE

The effects of varying impeller tip clearance on the performance of the NASA HECC impeller are presented in terms of impeller total pressure ratio (TPR), impeller total temperature rise ratio (TTR), and impeller efficiency (η) in Figure 3, Figure 4, and Figure 5, respectively. The performance metrics are calculated according to equations (1), (2), and (3):

$$TPR = \frac{P_{03}}{P_{00}}, \tag{1}$$

$$TTR = \frac{T_{03} - T_{00}}{T_{00}}, and \tag{2}$$

$$\eta = \frac{h_{03s} - h_{00}}{h_{03} - h_{00}}, \tag{3}$$

where P_0 is the stagnation pressure, T_0 is the stagnation temperature, and h_0 is the stagnation enthalpy. Furthermore, the subscripts 0 and 3 indicate the inlet rating plane and impeller exit rating station, respectively, consistent with the nomenclature in Figure 1, and the s subscript indicates the stagnation enthalpy for the isentropic compression process.

Data were acquired from 75% to 100% corrected speed from open-throttle to near-stall conditions. To preserve the integrity of the plastic transition duct configuration, speedline data acquisition was terminated prior to the onset of instability. Emphasis was placed on the higher speed portions of the map, and as such, 4.9% tip gap data were acquired only at 100% corrected speed and only two clearance conditions were investigated at 75% speed, the lowest speed considered.

The total pressure ratio of the stage decreases with increasing tip clearance, Figure 3, and the loss of total pressure between the tip gap settings increases with increasing corrected speed. There is negligible change in total pressure ratio between the 2.0% and 3.0% tip gap conditions at 75% corrected speed, but nearly a 3% decrement in total pressure ratio throughout most of the 100% characteristic. As the inducer approaches choke at 100% corrected speed, the characteristics converge to more similar operating conditions. Since the inducer tip clearance is nearly constant for all of the exit tip clearance set points, convergence to a choke mass flow rate dictated by the inducer is expected.

In contrast to total pressure ratio, the work input by the impeller does not change significantly with variation of tip clearance. In fact, the total temperature rise ratio is within the measurement uncertainty (which is less than 1%) for comparable operating conditions at different tip gaps. The minimal effect of tip clearance on work input is in agreement with past investigations in the literature [3–5]. However, it should be noted that the more detailed impeller exit survey data presented in Section 4 show evidence of variations in the work input that are

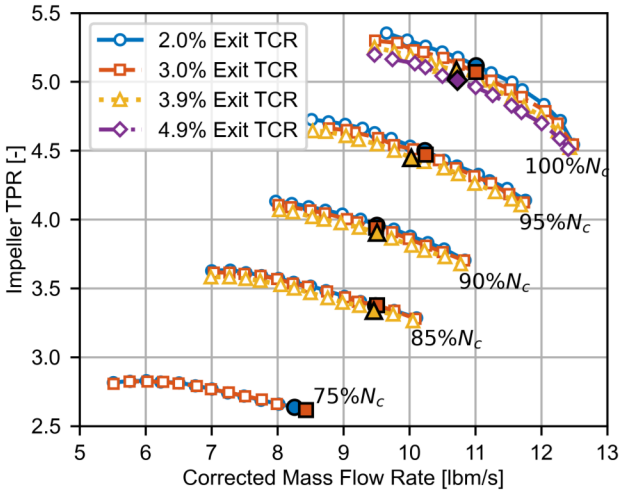

FIGURE 3. HECC IMPELLER TOTAL PRESSURE RATIO MAP FOR VARIOUS TIP CLEARANCE CONDITIONS WITH OPERATING POINTS MATCHED BY LOADING FACTOR INDICATED WITH FILLED SYMBOLS.

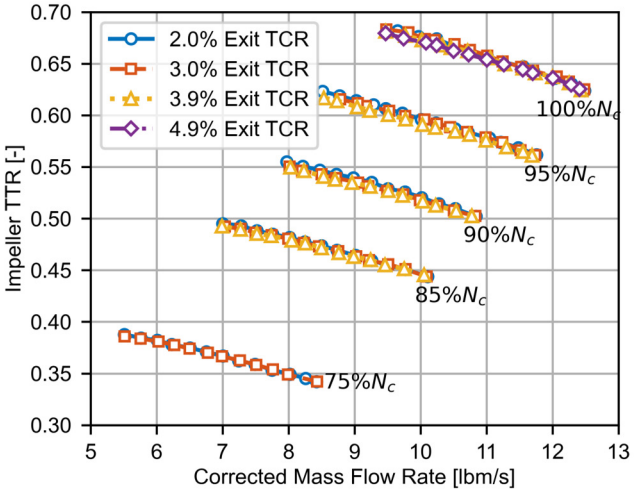

FIGURE 4. HECC IMPELLER WORK INPUT MAP FOR VARIOUS TIP CLEARANCE CONDITIONS.

not apparent from the overall performance results presented in Figure 4.

The decrement in total pressure ratio and lack of change in work input with increasing tip clearance naturally leads to reduced efficiency with increasing tip clearance, Figure 5. Due to the crowding of speedlines that often occurs in efficiency maps, only the 100% characteristic is shown. At the design operating point of 11-lbm/s, a 1.5-point drop in efficiency was observed from the design tip clearance to the largest tip clearance condition of 4.9%. The speedline for each tip gap setting is quite similar in shape but offset in magnitude with the speedlines

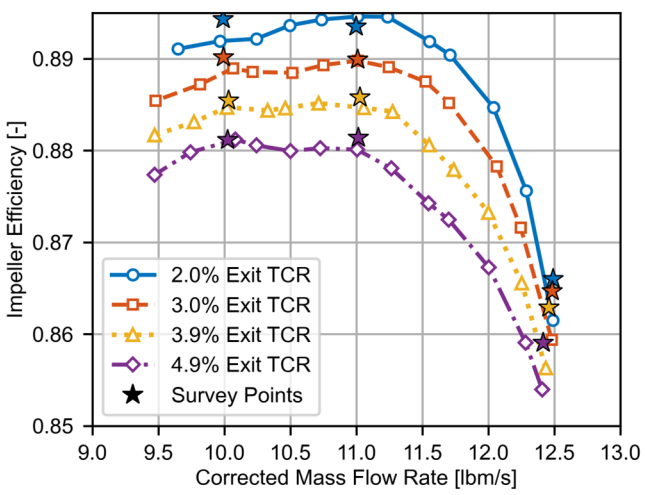

FIGURE 5. EFFECT OF TIP CLEARANCE ON HECC IMPELLER EFFICIENCY MAP AT 100% CORRECTED SPEED WITH IMPELLER EXIT SURVEY POINTS INDICATED.

converging towards the high flow side of the map as inducer choke is approached. While not shown here, the efficiency penalty from increased tip clearance increases with increasing speed similar to the behavior observed in the total pressure ratio map.

To more directly observe the effects of the tip gap variation on the compressor performance, the sensitivity of parameters of interest can be calculated from

$$-\Delta B = k\Delta CR \tag{4}$$

where B is the performance metric, k is the sensitivity of the specified metric, and CR is the tip clearance ratio. The tip clearance ratio is a nondimensional measure of tip clearance obtained by dividing the measured exducer tip clearance by the impeller exit blade height. For proper evaluation of the performance metrics, comparable operating points for each different tip clearance must be selected. As discussed by Fuehne et al. [6], matching inlet corrected mass flow rate at different tip gaps may result in different loading conditions and skew interpretation of results. They found that the loading factor parameter $TPR/\dot{m}_c$ results in the optimum comparison between tip clearances because the loading factor most closely matched operating conditions by allowing for selection of points along an operating line. For the present analysis, the peak efficiency point on each speedline at the design tip clearance (2.0%) was chosen as the reference condition. At each additional tip clearance, comparable operating points were matched based on the closest value of the loading parameter. The resulting matched points used for the calculations in equation (4) are represented by the larger, filled symbols in Figure 3.

After identification of the comparable operating points on each speedline, and with the knowledge that past research has

shown performance metrics have a linear relationship with the size of the tip clearance gap [3–6,8,16], a linear regression analysis was conducted. A value for the performance metric of interest at a theoretical "zero-clearance" operating condition was then extrapolated from equation (4) to determine the ideal value for the metric of interest. Finally, the change in the performance metric relative to the theoretical zero clearance can be obtained to explicitly consider the performance penalty to the performance parameter as a function the tip clearance ratio. The results of this analysis for the impeller total pressure ratio and impeller efficiency are presented in Figure 6 and Figure 7, respectively. Each figure includes experimental data as well as the linear relationship resulting from the regression analysis.

The penalty to the total pressure ratio increases linearly with increasing tip clearance ratio. The relationship is approximately linear with high coefficients of determination for all investigated speedlines; the lowest value for the coefficient of determination is 0.95. The impeller total pressure rise generally becomes more sensitive to increasing tip clearance as the tip clearance ratio increases. The 75% characteristic is a slight exception to this observation. The authors considered that this could be due to matching a peak efficiency point so near the high flow side of the speedline, but consideration of additional points along the characteristic near peak efficiency yielded similar sensitivities.

The impeller efficiency drop is nearly exactly linear for all considered speedlines, Figure 7. The lowest coefficient of determination of the matched points within the considered speedlines is 0.999 reinforcing the historical observation of linearly increasing performance penalties observed in the open literature [4–8]. In contrast to the impeller total pressure ratio, the sensitivity of the impeller efficiency decreases with increasing speed, with the exception of the 75% speedline.

In addition to the experimental data and regression analysis conducted on HECC, Figure 7 also includes lines indicating typical high and low values for the sensitivity of centrifugal compressor stage efficiency to the tip clearance ratio as determined by Lou et al. [16]. The high and low slopes were determined by analyzing 10 centrifugal compressors in the open literature, and results from the present analysis fit well within the range observed by Lou et al.

4. TIP CLEARANCE AND IMPELLER EXIT FLOW

Extensive impeller exit survey data acquired 107.2% of the impeller exit radius at 100% corrected speed are presented in Figure 8. Each row of Figure 8 is a distinct operating condition such that (a), (b), and (c) were recorded at near-stall, (d), (e), and (f) were recorded at peak efficiency, and (g), (h), and (i) were recorded at open throttle. The operating conditions for each survey in Figure 8 are indicated by the stars in Figure 5, and the colors used to indicate the different tip clearance gaps are consistent between the figures. It should be noted that the differences in efficiency between the survey points and the standard speedline points is due to the removal of two of the impeller total pressure rakes to install the survey probes in their place. The calculation of total pressure ratio, and thereby

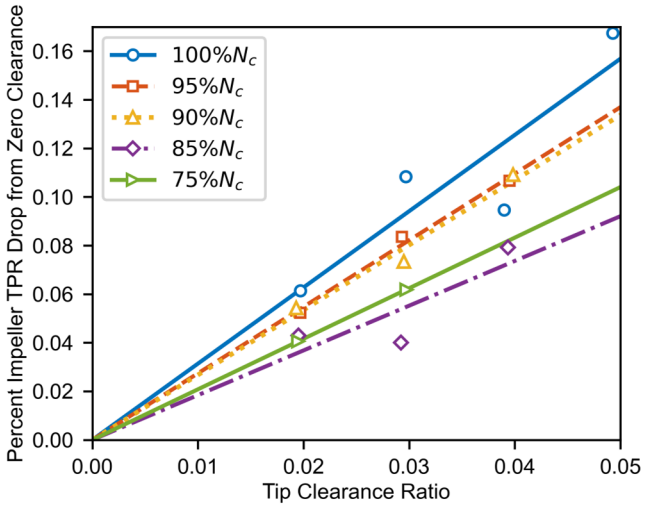

FIGURE 6. SENSITIVITY OF IMPELLER TOTAL PRESSURE RATIO TO TIP CLEARANCE IN PERCENT TPR DROP FROM THE IDEAL CONDITION.

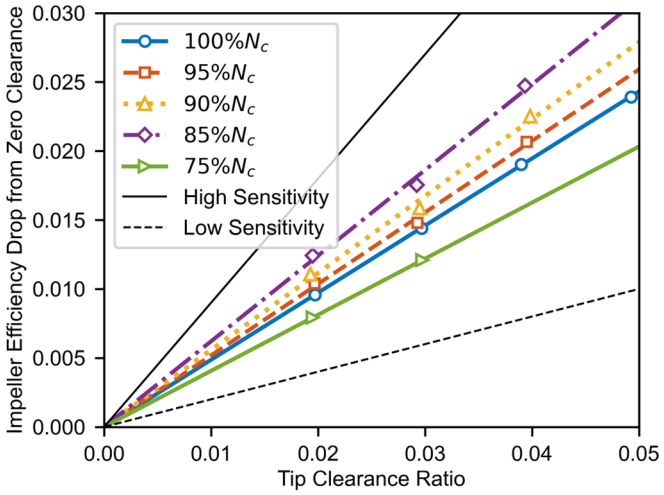

FIGURE 7. HECC IMPELLER EFFICIENCY DROP AS A FUNCTION OF TIP CLEARANCE WITH TYPICAL HIGH AND LOW RANGE OF SENSITIVITY INDICATED [16].

efficiency, slightly differs because of the change in instrumentation when the survey probes are installed.

Each column of Figure 8 is a different measurement quantity plotted as a function of spanwise location. Figure 8 subfigures (a), (d), and (g) present absolute flow angle relative to the tangential direction, (b), (e), and (h) present the total pressure ratio, and (c), (f), and (i) present the total temperature rise ratio. The range of the abscissa is kept constant in each column to allow for comparisons of the flow quantities between operating conditions, and the legend indicating the tip clearance gap size is consistent across all of the subfigures. Flow turning at the impeller exit increases (the impeller exit flow angle becomes more tangential) with decreasing mass flow rate (moving from

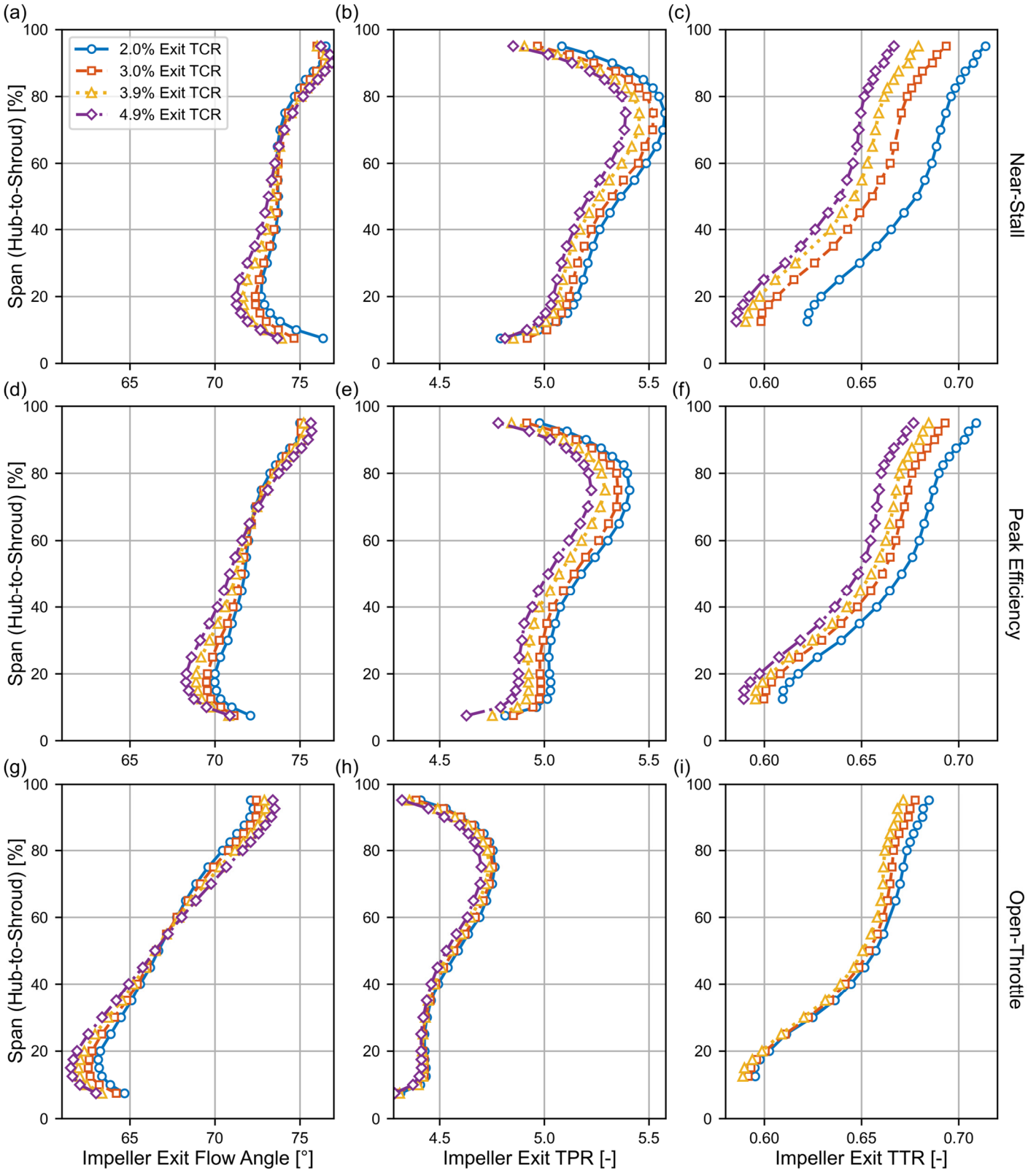

FIGURE 8. IMPELLER EXIT FLOW ANGLE, TOTAL PRESSURE RATIO, AND TOTAL TEMPERATURE RISE RATIO AT NEAR-STALL, PEAK EFFICIENCY, AND OPEN-THROTTLE OPERATING CONDITIONS FOR ALL ACQUIRED TIP CLEARANCES.

open throttle to peak efficiency to near-stall), Figure 8 (a), (d), and (g). Notably, flow turning increases nearly 10° from open throttle to near-stall in the 40% of the span nearest the hub while turning increases only 5° in the near-shroud region. Additionally, the variation of flow angle along the span decreases with increasing loading: the range of the flow angle decreases from nearly 10° to less than 5° from open throttle to near-stall, though most of the collapse in the range occurs between the open throttle and peak efficiency point. Increasing the tip clearance gap has a mixed impact on the impeller exit flow angle. The variation in the flow angle across the span increases with increasing tip gaps at all operating conditions. Interestingly, the size of the tip gap appears to have the smallest effect on the flow angle near the shroud and the greatest effect in the bottom half the span. This may not be the case for the 5% of the span nearest the shroud wall, but the proximity of the wall to the three-hole probe invalidated measurements in this region. Regardless, the numerical results will be used in the forthcoming discussion to ascertain why the size of the tip gap affects the bottom half of the impeller exit span.

As expected, total pressure ratio also increases with increasing loading, as shown in Figure 8 (b), (e), and (h). Unlike flow angle, however, the total pressure increases uniformly across the span and the range between the minimum and maximum value increases with decreasing mass flow rate. The shape of the total pressure profile is also similar across operating conditions. At all operating conditions, the total pressure decreases uniformly across the span with increasing tip clearance, though the effect of the tip gap size is more pronounced at the peak efficiency and near-stall points.

Relative to the impeller exit flow angle and total pressure ratio, the total temperature rise ratio does not appear to change as significantly with loading across the 100% speedline, Figure 8 (c), (f), and (i). This is at least partially due to the large variation of total temperature rise ratio across the span. The maximum variation in total temperature rise from hub to shroud is more than 150% of the increase in total temperature rise ratio from open-throttle to near-stall, Figure 4. Regardless, the work input increases fairly uniformly across the span with increasing loading and there is little change in the shape of the profile or range between the minimum and maximum values. The effect of the tip clearance gap on work input is more easily discernible via comparison of the impeller exit surveys than in the work input map in shown Figure 4. The penalty to the work input from increasing tip gap sizes penetrates to lower spans with increasing loading, and at peak efficiency and near-stall conditions the loss of work input appears to decrease slightly as the tip gap increases. The reduction in work input with increasing tip gap size at least partially accounts for the reduction in total pressure: less total pressure rise can be achieved since less work is done on the flow by the impeller.

All of the experimental data presented in the present work, including the impeller exit surveys, as well as static pressure measurements throughout the flow path, have been made available in the HECC Data Archive [13]. At the time of writing, this is the most extensive centrifugal compressor tip clearance data set available in the open literature.

5. IMPELLER FLOW FIELD ANALYSIS

A steady-state full stage computational model for the HECC vaneless diffuser configuration was developed to support this study. AeroDynamic Solutions code WAND was used to generate the mesh and the simulations were run with the solver LEO [17]. The Wilcox k-ω 98 model with variable specific heat was used as the turbulence model for all simulations [18]. The impeller mesh was generated from blade sections extracted from the solid model of the component available on the HECC Data Archive [13]. Inputs to the model included the design point mass flow rate, design point rotational speed, and standard day inlet conditions. Tip clearance measurements taken in the experiment were also specified at the inducer, knee, and exducer for each case investigated. The flow field in the tip gap region was discretized with 17 points in the span-wise direction. A grid independence study was conducted with four meshes, with the finest mesh having a nodal count of 2,794,519. Based on this study, a mesh with 2,027,603 nodes was selected for the investigation. Additional specifics of the model are detailed in Part 1.

Prior to using the numerical model for investigation of tip clearance effects, the model was validated for use in the analysis of the tip clearance flow at each experimental tip gap setting. Simulations were conducted from near choke to near-stall at each tip clearance condition. None of the speedlines presented herein were throttled to the onset of numerical instability. As such, the differences observed in the numerical results at the low flow rate side of the 100% speedline are artifacts from the generation of speedlines at different mass flow rates and are not significant.

The numerical model accurately captured the shift in the design speed characteristic due to the increasing tip clearance, Figure 9. The model tended to overpredict the impeller TPR for each case, though the magnitude of the over prediction decreased at the high flow side of the speedline. Most importantly, the decrement in total pressure ratio as a result of increasing tip clearance was accurately captured by the model. Moreover, the differences in the impeller exit flow features between each tip clearance at the design mass flow rate were also well represented by the numerical model, Figure 10. For each tip clearance, the model overpredicted the impeller exit total pressure ratio between the hub and 60% span and underpredicted the metric above 60% span, but the difference in total pressure ratio between each tip clearance condition was accurately captured. Since the model captured the effects of changing tip clearance on both the one-dimensional impeller performance as well as the exit flow field with high fidelity, it was deemed to be fit for use in further analysis of the impeller flow field in conjunction with the experimental data.

While the measurements in Figure 8 are extensive, the analysis of these experimental data are primarily observational: they answer the question, “How does changing tip clearance affect the impeller exit flow?” To answer the question, “Why does increasing tip clearance have these effects on the impeller

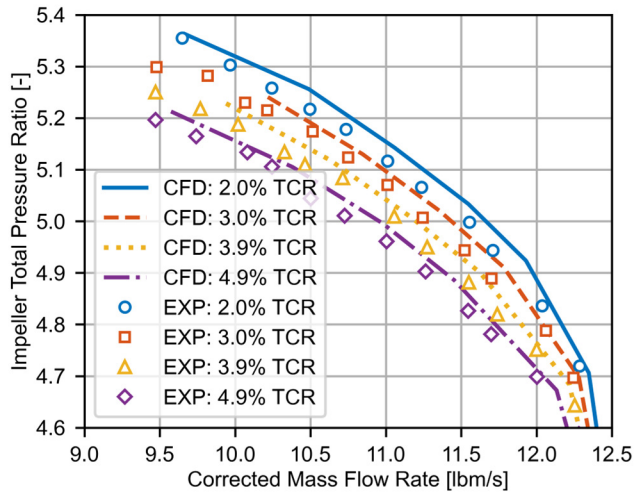

FIGURE 9. MEASURED AND CALCULATED HECC IMPELLER EXIT TOTAL PRESSURE RATIO AT 100% CORRECTED SPEED.

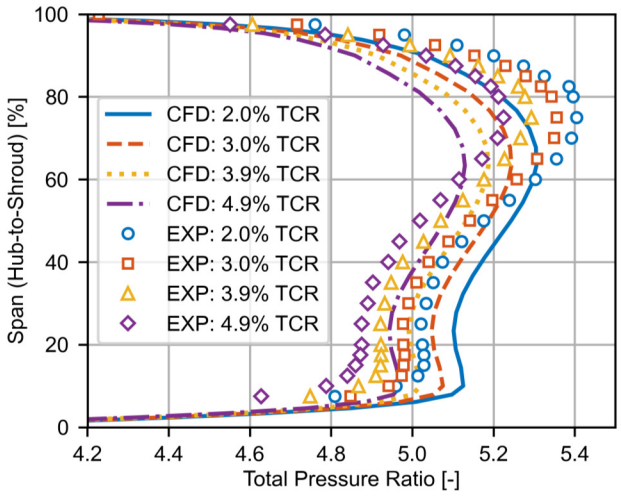

FIGURE 10. SPAN-WISE VARIATION OF MEASURED AND CALCULATED IMPELLER EXIT TOTAL PRESSURE RATIO.

exit flow?" validated numerical simulations are interrogated alongside the experimental data. Meridional mass averages of the turbulence kinetic energy (TKE) in exducer flow field for each of the tip clearances of interest are presented in Figure 11 at the design conditions for the impeller (100% corrected speed, 11-lbm/s). The gridlines in the meridional view are spaced from 0%-100% across the span and meridional directions at 20% and 4% increments, respectively. The percent meridional length of the impeller domain has been demarcated on the (a) subfigures for clarity. The thick dashed-white line indicates the impeller trailing edge radius, and the scale in the color map is consistent across all four subfigures.

At all considered tip clearance gaps, the highest levels of TKE in the impeller (indicated by red levels in the contour plots in Figure 11) occur in the tip clearance gap between the rotating impeller and stationary shroud. However, as the tip clearance increases, the initial peak levels of TKE move upstream from approximately 76% of impeller meridional length at design tip clearance (Figure 11a) to 68% of the meridional length at 4.9% TCR (Figure 11d). Moreover, the high TKE levels penetrate further across the passage towards the hub both upstream and downstream of the impeller trailing edge. The high TKE band is limited to the 20% of the span nearest the shroud at the 2.0% tip gap, but it increases in breadth to encompass 30% or more of the near-shroud portion passage at the 4.9% tip clearance condition. As the tip clearance increases from the design gap of 2.0% to 4.9%, high levels of TKE occur further upstream and penetrate further across the span. Additionally, the transition region between relatively high and low TKE levels (white in the contour plot) also begins further upstream and increases in spanwise breadth.

The increase in the turbulence kinetic energy along the shroud with increasing tip clearance corresponds to increased entropy generation in the tip region, Figure 12. The gridlines and impeller trailing edge are demarcated in the same manner as Figure 11, and the scale of the colormap in Figure 12 is consistent across the subfigures. Losses in the tip gap region are the dominant contributors to entropy generation within the impeller, and the size of the high entropy region increases as the tip gap increases. The highest entropy levels occur along the shroud and penetrate to approximately 25%, 30%, 35%, and 40% of the span at the impeller trailing edge for the 2.0%, 3.0%, 3.9%, and 4.9% cases, respectively. Unlike TKE, the upstream entropy levels are quite similar at each tip clearance.

Together, Figure 11 and Figure 12 provide insight into the processes in the impeller that affect the impeller exit flow field. High levels of TKE are generated in the tip gap (Figure 11) and lead to two outcomes with respect to the size of the tip clearance gap. First, the increased TKE in the larger tip gaps directly leads to greater levels of entropy generation both within and just downstream of the impeller passage as turbulence is dissipated as heat. Second, the increased TKE within the passage appears to propagate increased spanwise mixing within the impeller passages, and the relatively high loss flow near the tip penetrates further across the passage from the gap region. The increased permeation of high loss flow across the impeller span at larger tip gaps reduces the useful work input provided by the impeller which can be directly observed in Figure 13.

In Figure 13, contours of the normalized isentropic efficiency at the impeller trailing edge for each tip gap setting are presented. The values for efficiency are calculated relative to the stage inlet conditions (standard day). Additionally, each efficiency contour has been normalized by the overall impeller efficiency at the local tip clearance conditions to remove the confounding effect of comparing the contours between different operating conditions. At design tip clearance, Figure 13a, a band of low efficiency is present near the shroud in both passages. Perhaps unexpectedly, the band of low efficiency fluid decreases

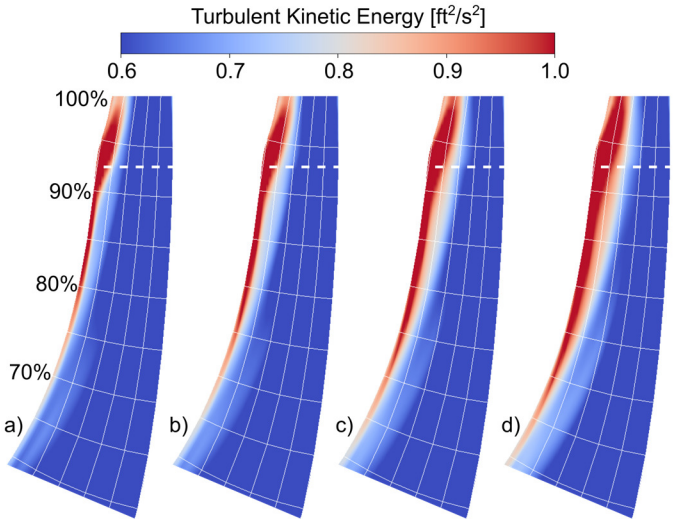

FIGURE 11. MERIDIONAL VIEW OF MASS AVERAGED TURBULENCE KINETIC ENERGY IN THE EXDUCER AT (A) 2.0%, (B) 3.0%, (C) 3.9%, AND (D) 4.9% TIP GAP RATIOS.

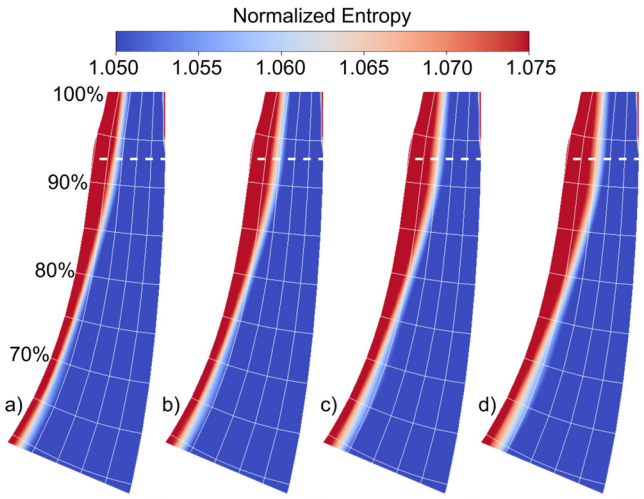

FIGURE 12. MERIDIONAL VIEW OF MASS AVERAGED ENTROPY NORMALIZED BY THE INLET CONDITIONS IN THE EXDUCER AT (A) 2.0%, (B) 3.0%, (C) 3.9%, AND (D) 4.9% TIP GAP RATIOS.

in size as the tip gap increases, but it also becomes less localized to the tip region due to greater mixing from higher TKE levels. Additionally, the range of the efficiency observed across the passage steadily decreases across all four tip clearance conditions, a further indication of increased mixing as the high and low efficiency regions coalesce to values between the extremes. This mixing moderates the losses nearest the shroud but allows the high entropy flow to permeate the passage. As such, the peak efficiency region (outlined by the white dashed lines in each subfigure) decreases in size in both the main-splitter and splitter-main passages: at 2.0% the peak normalized efficiency occupies nearly a third of the passage but is almost eliminated at 4.9%. These computational results give some insight into impeller exit flow measurements acquired at the design point presented in Figure 8 (d), (e), and (f). The low momentum fluid near the shroud is convected towards the near-hub half of the span at larger tip gaps which reduces the flow turning by the impeller at and below 60% span (Figure 8d).

The low efficiency region near the shroud in Figure 13 can be inferred from comparison of the TPR and TTR surveys in Figure 8e and Figure 8f. Regardless of the tip gap size, TPR is lowest in the top 85% of the span while the TTR is at its greatest in the same region. Additionally, it appears that the TPR decreases more rapidly and TTR increases more rapidly near the shroud as tip clearance increases, also indicating smaller efficiency minima occur near the shroud at small tip gap sizes. Finally, convection of the high loss fluid near the shroud across the passage decrements TPR at a greater rate than the TTR needed to maintain the same level of efficiency, and thus the breadth and magnitude of the high efficiency region in Figure 13a decreases with increases in tip clearance.

6. CONCLUSIONS

Flow phenomena associated with the tip gap between rotating and stationary components are major contributors to loss generation in compressors, and tip clearance flow losses have taken on greater and greater importance as gas turbines have decreased in size while tip clearance gaps have had to remain constant. As such, understanding the production of losses associated with the tip clearance flow is critical to improving the efficiency of future gas turbine compressors. To provide insight into these phenomena, a comprehensive experimental and numerical investigation of tip clearance effects was conducted at the NASA Glenn Research Center utilizing the vaneless diffuser configuration of the High Efficiency Centrifugal Compressor.

Aerodynamic performance data were collected at four different tip gaps ranging from 0.012-in to 0.030-in, which correspond to tip gap ratios from 2.0% to 4.9%, at 75%, 85%, 90%, 95%, and 100% corrected speed from open-throttle to near-stall conditions. The performance of the impeller decreased with increasing tip gap sizes in all major metrics, though the effect on work input was least distinguishable. Additionally, the performance penalty to the impeller TPR and efficiency were linear with the tip gap ratio at all considered speeds with high values for the coefficient of determination (>0.95).

Three-hole and total temperature probe measurements acquired across the span just downstream of the impeller trailing edge were used to quantify the impeller exit flow angle, total pressure ratio, and work input in detail at open-throttle, peak efficiency, and near-stall on the 100% characteristic. Impeller flow turning decreased in the bottom half of the span with increasing tip clearance, while total pressure and total temperature decreased more uniformly along the span, although the range between the minimum and maximum TTR values across the span also increased with increasing tip clearance. The

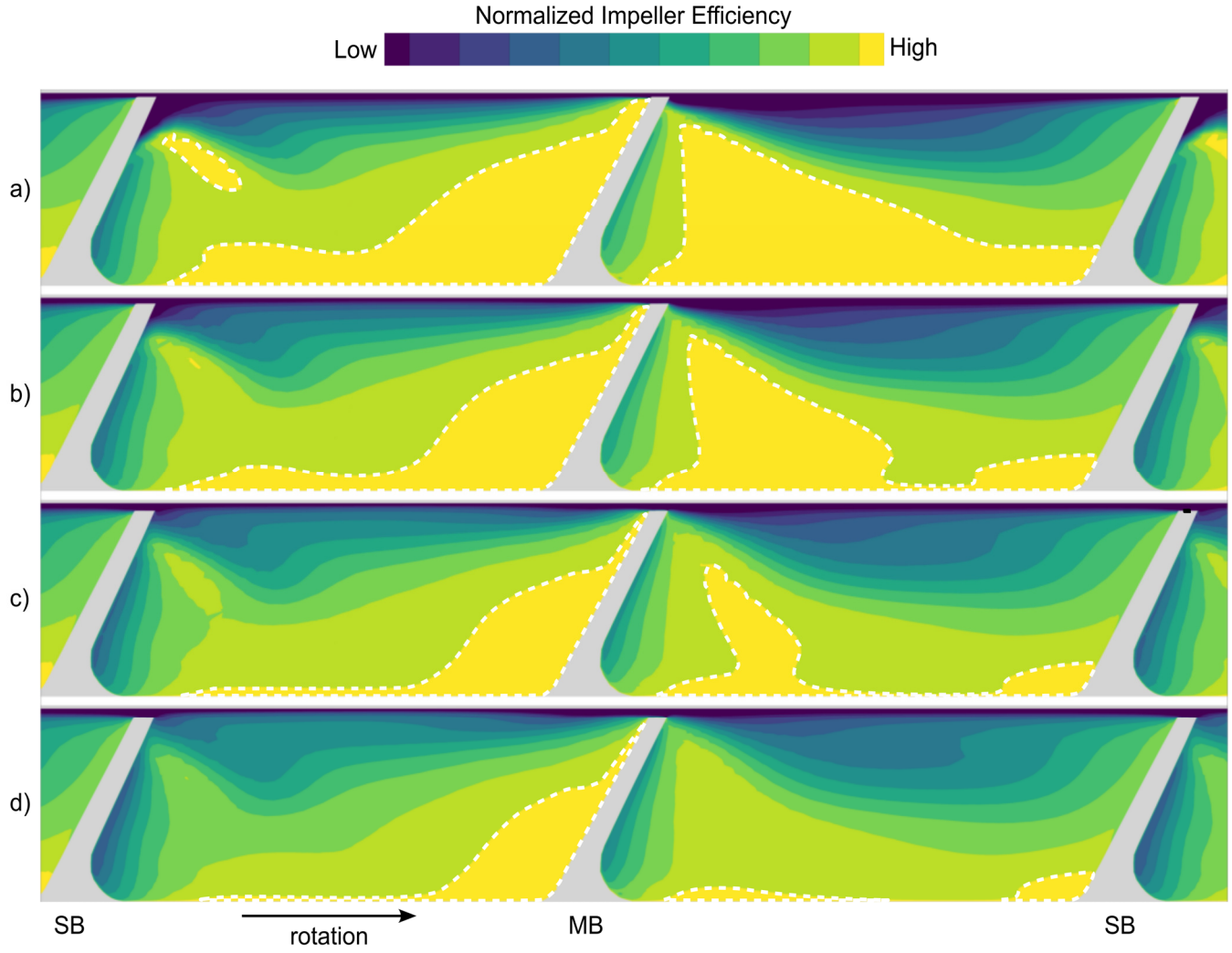

FIGURE 13. CONTOURS OF IMPELLER EFFICIENCY NORMALIZED BY THE LOCAL OPERATING POINT FOR (A) 2.0%, (B) 3.0%, (C) 3.9%, AND (D) 4.9% TIP GAP RATIOS WITH THE PEAK EFFICIENCY REGION OUTLINED BY DASHED WHITE LINES.

aerodynamic performance data as well as the impeller exit surveys have been made available on the HECC Data Archive at https://storage.googleapis.com/hecc-data/NASA-HECC-Data-Archive.zip which, to the authors' knowledge, is the most extensive centrifugal compressor tip clearance dataset available in the open literature [13].

Numerical simulations were validated at peak efficiency on the 100% speedline for each of the four tip gap measurements. The simulations were found to accurately capture the effect of tip clearance variation on the impeller performance and, as such, were used to give insight into the fluid phenomena that caused the performance penalties and variation in impeller exit measurements. At larger tip gaps, increased levels of turbulence kinetic energy near the shroud led to increased entropy generation and spanwise mixing which impeded pressure rise across the span as tip clearance increased. Moreover, the high loss fluid propagated across the span and reduced the efficiency of work input throughout the passage.

The observations and trends documented in the present work are in good agreement with past investigations. In conjunction with other works in the open literature, future centrifugal compressor designs can leverage the information that increased spanwise mixing is a major contributor to increasing tip clearance losses at larger tip gaps.

ACKNOWLEDGEMENTS

This effort is sponsored by both the NASA Transformational Tools and Technologies Project and the NASA Revolutionary Vertical Lift Technology Project. The authors would like to thank Mr. Alex Camargo, Mr. Jacob Jaksic, Mr. Matthew Blaha, and Mr. Jonathan Mitchell for their help conducting experiments in the NASA Small Engine Components Compressor Test Facility. The authors are also grateful to Mr. Michael Ni and Mr. Gregorio

Robles Vega for their assistance in developing the computational models.

REFERENCES

[1] Senoo, Y., and Ishida, M., 1987, "Deterioration of Compressor Performance Due to Tip Clearance of Centrifugal Impellers," Journal of Turbomachinery, **109**(1), pp. 55–61.

[2] Brasz, J. J., 1988, "Investigation Into the Effect of Tip Clearance on Centrifugal Compressor Performance," *Volume 1: Turbomachinery*, American Society of Mechanical Engineers, Amsterdam, The Netherlands, p. V001T01A066.

[3] Ishida, M., Senoo, Y., and Ueki, H., 1990, "Secondary Flow Due to the Tip Clearance at the Exit of Centrifugal Impellers," Journal of Turbomachinery, **112**(1), pp. 19–24.

[4] Tang, J., Turunen-Saaresti, T., Reunanen, A., Honkatukia, J., and Larjola, J., 2006, "Numerical Investigation of the Effect of Tip Clearance to the Performance of a Small Centrifugal Compressor," *Volume 5: Marine; Microturbines and Small Turbomachinery; Oil and Gas Applications; Structures and Dynamics, Parts A and B*, ASMEDC, Barcelona, Spain, pp. 411–418.

[5] Wilkosz, B., Kunte, R., Schwarz, P., Jeschke, P., and Smythe, C., 2014, "Numerical and Experimental Investigation of an Impeller Tip Clearance Variation in an Aero-Engine Centrifugal Compressor with Close-Coupled Pipe-Diffuser," CEAS Aeronaut J, **5**(2), pp. 171–183.

[6] Fuehne, M. F., Lou, F., and Key, N. L., 2022, "Experimental and Numerical Investigation of Clearance Effects in a Transonic Centrifugal Compressor," Journal of Propulsion and Power, pp. 1–11.

[7] Eum, H.-J., and Kang, S.-H., 2002, "Numerical Study on Tip Clearance Effect on Performance of a Centrifugal Compressor."

[8] Turunen-Saaresti, T., and Jaatinen, A., 2013, "Influence of the Different Design Parameters to the Centrifugal Compressor Tip Clearance Loss," Journal of Turbomachinery, **135**(1), p. 011017.

[9] Mashimo, T., Watanabe, I., and Ariga, I., 1979, "Effects of Fluid Leakage on Performance of a Centrifugal Compressor," Journal of Engineering for Power, **101**(3), pp. 337–342.

[10] Senoo, Y., and Ishida, M., 1986, "Pressure Loss Due to the Tip Clearance of Impeller Blades in Centrifugal and Axial Blowers," Journal of Engineering for Gas Turbines and Power, **108**(1), pp. 32–37.

[11] Medic, G., Sharma, O. P., Jongwook, J., Hardin, L. W., McCormick, D. C., Cousins, W. T., Lurie, E. A., Shabbir, A., Holley, B. M., and Van Slooten, P. R., 2017, *High Efficiency Centrifugal Compressor for Rotorcraft Applications*, E-18856-1.

[12] Harrison, H. M., McNichols, E. O., and Blaha, M. R., 2023, "NASA Small Engine Components Compressor Test Facility: High Efficiency Centrifugal Compressor Vaneless Diffuser and Transition Duct Configurations," *Boston, MA*, American Society of Mechanical Engineers Digital Collection.

[13] Harrison, H. M., 2022, "NASA HECC Data Archive," NASA [Online]. Available: https://storage.googleapis.com/hecc-data/NASA-HECC-Data-Archive.zip.

[14] Treaster, A. L., and Yocum, A. M., 1978, *The Calibration and Application of Five-Hole Probes*, PENNSYLVANIA STATE UNIV UNIVERSITY PARK APPLIED RESEARCH LAB.

[15] Sitaram, N., Lakshminarayana, B., and Ravindranath, A., 1981, "Conventional Probes for the Relative Flow Measurement in a Turbomachinery Rotor Blade Passage."

[16] Lou, F., Fabian, J. C., and Key, N. L., 2019, "Design Considerations for Tip Clearance Sensitivity of Centrifugal Compressors in Aeroengines," Journal of Propulsion and Power, **35**(3), pp. 666–668.

[17] "ADSCFD," Aerodynamic Solutions, San Ramon, CA USA.

[18] Wilcox, D. C., 2006, *Turbulence Modeling for CFD*, D C W Industries, La Cañada, Calif.